arXiv:1202.3165v3 [hep-ph] 9 Mar 2012

Preliminary results from the 4PI Effective Action

M.E. Carrington* and Wei-Jie Fu†
Department of Physics, Brandon University, Brandon, Manitoba, R7A 6A9 Canada and
Winnipeg Institute for Theoretical Physics, Winnipeg, Manitoba
(Dated: March 13, 2012)

We study the renormalizability of the 4-Loop 4PI effective action in a symmetric scalar theory with quartic coupling. We show that the self-consistently determined 2-point and 4-point functions can be renormalized using a coupling constant counter-term in the Lagrangian of the original theory. We do a numerical lattice calculation to obtain solutions in a toy 2-dimensional model. The self-consistent solutions for the 2-point and 4-point functions agree well with the perturbative ones when the coupling is small. When the coupling is large, perturbative calculations break down, but the self-consistent solution is well behaved.

PACS numbers: 11.15.Tk, 11.10.Gh, 11.10.-z, 11.10.Kk

I. INTRODUCTION

The resummation of certain classes of Feynman diagrams to infinite loop order is a powerful method in quantum field theory. A well known example is the hard thermal loop theory [1], developed in the context of thermal field theory, which resums all loop corrections which are of the same order as tree diagrams, when external momenta are soft.

In recent years, another kind of resummation approach, known as two-particle irreducible (2PI) effective action theory, has attracted a lot of attention. In the 2PI formalism, the effective action is expressed as a functional of the non-perturbative propagator [2, 3], which is determined through a self-consistent stationary equation after the effective action is expanded to a certain order in the loop or $1/N$ expansion. This self-consistent equation of motion resums certain classes of diagrams to infinite order. The classes that are resummed are determined by the set of skeleton diagrams that are included in the truncated effective action. Numerical studies indicate that the 2PI effective action theory is very successful in describing equilibrium thermodynamics, and also the quantum dynamics of far from equilibrium of quantum fields. The entropy of the quark-gluon plasma obtained in the 2PI formalism shows very good agreement with lattice data for temperatures above twice the transition temperature [4]. The poor convergence problem usually encountered in high-temperature resummed perturbation theory with bosonic fields is also solved in the 2PI effective action theory [5]. Furthermore, it has been shown that non-equilibrium dynamics with subsequent late-time thermalization can be well described in the 2PI formalism (see [6] and references therein). The 2PI effective action has also been combined with the exact renormalization group to provide efficient non-perturbative approximation schemes [7]. The shear viscosity in the $O(N)$ model has been computed using the 2PI formalism [8].

The 2PI effective action theory has its own drawbacks and limitations. When the effective action is expanded to only 2-loops, the 2PI effective action is complete. However, when the expansion is beyond 2-loops, one must use a higher order effective theory to obtain a complete description [9]. Higher order effective theories are defined in terms of self-consistently determined n-point functions for $n > 2$. It has been shown that the 2PI effective action is insufficient to calculate transport coefficients for high temperature gauge theories [10], but that higher order nPI effective actions can be used [11].

---

* carrington@brandonu.ca
† fuw@brandonu.ca

The 4PI effective action for scalar field theories is derived in Ref. [12] using Legendre transformations. The method of successive Legendre transforms is used in [9, 13]. A new method has been developed to calculate the 5-loop 5PI and 6-loop 6PI effective action for scalar field theories [14, 15]. The 3PI and 4PI effective actions have been used to obtain a set of integral equations from which the leading order and next-to-leading order contributions to the viscosity can be calculated [16, 17].

A lot of effort has been devoted to numerical computations in 2PI theories. For higher order nPI theories, progress has been made in understanding the analytic structure of the theory, but no numerical calculations have been done. One reason is that the renormalizability of higher order nPI theories has not been proven. Another is that numerical calculations for higher order effective theories are much more difficult than the corresponding calculations with the 2PI effective theory. In this paper, we present some preliminary results from our attack on this problem. We work with a scalar field theory in the symmetric phase and use the 4PI effective action truncated at 4-Loops. The paper is organized as follows. In sections II and III we define our notation. In section IV we describe the technique we will use to manipulate divergent integrals. In sections V and VI we prove the renormalizability of the 4- and 2-point functions, respectively. In section VII we show that the coupling counter-terms obtained in the previous two sections which renormalize the 4- and 2-point functions are the same, to within the approximation order imposed by the truncation of the effective action. In section VIII we present some results from a numerical calculation in 2-dimensions, and in section IX we give our conclusions.

II. GENERAL FORMALISM

We consider the following Lagrangian:

$$\mathcal{L} = \frac{1}{2}(\partial_\mu\varphi\partial^\mu\varphi - m^2\varphi^2) - \frac{i\lambda}{4!}\varphi^4\,. \tag{1}$$

The classical action is:

$$\begin{aligned}
&S[\phi] = S_0[\varphi] + S_{\rm int}[\varphi]\,, &(2)\\
&S_0[\varphi] = \frac{1}{2}\int d^4x\, d^4y\, \varphi(x)[iG_0^{-1}(x-y)]\varphi(y)\,,\\
&S_{\rm int}[\varphi] = -\frac{i\lambda}{4!}\int d^4x\varphi^4(x)\,. &(3)
\end{aligned}$$

In most equations in this paper, we suppress the arguments that denote the space-time dependence of functions. As an example of this notation, the non-interacting part of the classical action is written:

$$\begin{aligned}
&S_0[\varphi] = \frac{1}{2}\int d^4x\, d^4y\, \varphi(x)[iG_0^{-1}(x-y)]\varphi(y) \quad\rightarrow\quad \frac{i}{2}G_0^{-1}\varphi^2\,, &(4)\\
&G_0^{-1} = -i\frac{\delta^2 S_{cl}[\varphi]}{\delta\varphi^2}\Big|_{\varphi=0} = i(\Box + m^2)\,.
\end{aligned}$$

The effective action is obtained from the Legendre transformation of the connected generating functional:

$$\begin{aligned}
&Z[R_1,R_2,R_3,R_4] = \int [d\varphi]\;{\rm Exp}[i\,(S_{cl}[\varphi] + R_1\varphi + \frac{1}{2}R_2\varphi^2 + \frac{1}{3!}R_3\varphi^3 + \frac{1}{4!}R_4\varphi^4)]\,, &(5)\\
&W[R_1,R_2,R_3,R_4] = -i\,{\rm Ln}Z[R_1,R_2,R_3,R_4]\,,\\
&\Gamma[\phi,G,V_3,V_4] = W - R_1\frac{\delta W}{\delta R_1} - R_2\frac{\delta W}{\delta R_2} - R_3\frac{\delta W}{\delta R_3} - R_4\frac{\delta W}{\delta R_4}\,.
\end{aligned}$$

Connected and proper green functions are denoted V_j^c and V_j respectively, where the subscript j indicates the number of legs. They are defined:

$$V_j^c = \langle \varphi^j \rangle_c = -(-i)^{j+1} \frac{\delta^j W}{\delta R_1^j} \,. \tag{6}$$

The equations that relate the connected and proper vertices are obtained from their definitions using the chain rule:

$$V_j = i\frac{\delta^j}{\delta\phi^j}\Gamma_{\rm 1PI} = i\frac{\delta^j}{\delta\phi^j}\left(W[R_1] - R_1\phi\right) \,. \tag{7}$$

We organize the calculation of the effective action using the method of subsequent Legendre transforms [9, 13]. This method involves starting from an expression for the 2PI effective action and exploiting the fact that the source terms R_3 and R_4 can be combined with the corresponding bare vertex by defining a modified interaction vertex. The result is:

$$\begin{aligned}
&\Gamma[\phi, G, V_3, V_4] = \frac{i}{2}G_0^{-1}\phi^2 + \frac{i}{2}{\rm Tr}\ln G^{-1} + \frac{i}{2}{\rm Tr}G_0^{-1}G + \Gamma_{\rm int}[\phi, G, V_3, V_4], \qquad (8)\\
&i\Gamma_{\rm int}[\phi, G, V_3, V_4] = \frac{\lambda}{4!}\phi^4 + \frac{\lambda}{4}(\phi^2 G) + \Phi_2[\phi, G, V_3, V_4] \,,
\end{aligned}$$

where $\Phi_2[\phi, G, V_3, V_4]$ represents diagrams with 2 and more loops.

A key point in the proof of renormalizability is the fact that there are different possible definitions of j-point functions for a given j. A general proof of renormalizability must demonstrate that all j-point functions are made finite by a set of momentum independent counter-terms which have the same structure as the terms in the original Lagrangian. Further, one must show that all j-point functions for a given j are made finite by the same counter-term, at a different level of truncation of the effective action. Equivalently, since the nPI effective theory coincides with the untruncated bare perturbative theory in the limit $n \to \infty$, the counter-terms of the effective theory and the bare theory must also coincide in this limit.

In this paper we consider only the self-consistent 2- and 4-point functions in the symmetric phase. These are obtained by solving simultaneously the equations of motion:

$$\frac{\delta\Gamma[\phi, G, V_3, V_4]}{\delta G}\Big|_{\phi=0, G=\tilde{G}, V_3=0, V_4=\tilde{V}_4} = 0 \,, \quad \frac{\delta\Gamma[\phi, G, V_3, V_4]}{\delta V_4}\Big|_{\phi=0, G=\tilde{G}, V_3=0, V_4=\tilde{V}_4} = 0 \,. \tag{9}$$

From now on we drop the subscript on the 4-point vertex function and write $V := V_4$ and $\tilde{V} := \tilde{V}_4$.

III. RENORMALIZATION

The variables m, λ, G and V in section II should all carry a subscript B to indicate that they are bare quantities. These bare quantities (with subscript B) are related to the renormalized ones by the following relations:

$$\begin{aligned}
&\delta m^2 = Z m_B^2 - m^2 \,, \quad \delta\lambda = Z^2\lambda_B - \lambda \,, \qquad (10)\\
&G_B = ZG \,, \quad V_B = Z^{-2}V \,,\\
&Z G_{0B}^{-1} = G_0^{-1} + \delta G_0^{-1} \,, \quad \delta G_0^{-1} = i(\delta Z \Box + \delta m^2) \,, \quad \delta Z = Z - 1 \,.
\end{aligned}$$

In order to simplify the notation we have not introduced a subscript R for renormalized quantities and suppressed the subscript B everywhere except in the equation (10). All quantities in section II are bare, and all quantities in all other sections are renormalized.

We consider the 4-loop 4PI effective action. We introduce a finite set of counter-terms with the same structure as the terms in the original action. The effective action expressed in terms of renormalized quantities is:

$$\begin{aligned} i\Gamma[G,V] &= -\frac{1}{2}\mathrm{Tr}\ln G^{-1} - \frac{1}{2}\mathrm{Tr}G_0^{-1}G + \Phi_{\rm int}[G,V]\,, \\ \Phi_{\rm int} &= \Phi_{\rm A} + \Phi_{\rm B}\,, \\ \Phi_{\rm A} &= -\frac{1}{2}\mathrm{Tr}\delta G_0^{-1}G + \frac{1}{8}(\lambda+\delta\lambda_{et})G^2 + \frac{1}{4!}(\lambda+\delta\lambda_{bb})G^4V\,, \\ \Phi_{\rm B} &= -\frac{1}{2}\frac{1}{4!}V^2G^4 + \frac{1}{48}V^3G^6\,. \end{aligned} \tag{11}$$

The functionals $\Phi_{\rm A}$ and $\Phi_{\rm B}$ are shown in figure 1.[1] In all diagrams, bare 4-vertices are represented by white circles, counter-terms are circles with crosses in them, and solid dots are the vertex V. The notation $\delta\lambda_{et}$ and $\delta\lambda_{bb}$ indicates the counter-terms associated with the bare vertices on the EIGHT and BBALL$_0$ diagrams, respectively. The subscripts are introduced only for notational convenience. In section VII we show that these counter-terms are the same, to within the approximation order of the skeleton expansion.

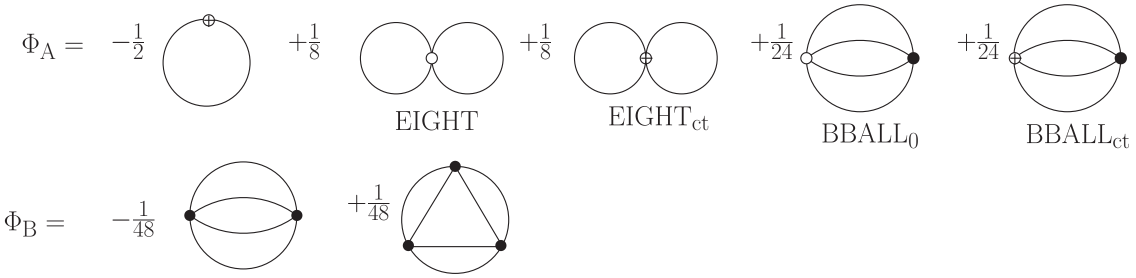

FIG. 1. The effective action at 4-Loops including counter-terms. The open circle is a bare vertex, the circle with a cross denotes a counter-term, and the proper vertex is indicated by a solid dot. We label the EIGHT and BBALL$_0$ diagrams, which contain a bare vertex, and the corresponding counter-terms.

IV. VERTEX SPLITTING

We want to remove divergences in the 2- and 4-point functions by adding counter-terms to the action. The first step is to manipulate the divergent integrals so they can be written as a sum of terms of the form:

$$\begin{aligned} I^{(1)} &= (\text{finite}) + (\text{overall } \vec{p}\text{-independent divergence}) \\ I^{(2)} &= (\text{finite}) + (\text{overall } \vec{p}\text{-independent divergence}) + (\text{overlapping divergences}) \end{aligned} \tag{12}$$

where the notation $I^{(x)}$ indicates an x-loop integral. An overlapping divergence appears in a multi-loop diagram when a sub-divergence is present. For the theory to be renormalizable, we must show that for all j-point functions, the overlapping divergences can be cancelled by counter-term insertions in lower loop integrals, and the overall momentum independent divergences can be absorbed by overall counter-terms.

---

[1] All figures are drawn using jaxodraw [18].

We start by defining some notation. We use the momentum variables:

$$L_t = L + K - P\,, \quad L_s = L + Q - P\,, \quad R_t = R + K - P\,, \quad Q_t = Q + K - P\,. \tag{13}$$

Since the vertex is symmetric, we can write the four momentum arguments in any order. We write all momenta arguments as incoming. We write propagator arguments as subscripts to save space: for example, $G(L) =: G_L$.

Now we discuss how to divide integrals into the form in equation (12). The basic strategy is as follows. We write some group of factors in the integrand as a function $f(\{P_i\}, L)$ with L an integration variable and $L \notin \{P_i\}$. Then we split the function f by writing:

$$f(\{P_i\}, L) = \Delta_L f + f(0, L) \;\; \text{with} \;\; \Delta_L f = f(\{P_i\}, L) - f(0, L)\,. \tag{14}$$

For large L we have $\Delta_L f \sim \frac{1}{L} f$. Using Weinberg's theorem we can show that the integrals we need to deal with are at most logarithmically divergent, and therefore a term that contains a factor $\Delta_L f \sim \frac{1}{L} f$ is finite when integrated over L.

Some of the diagrams we will need to consider are shown in figure 2.

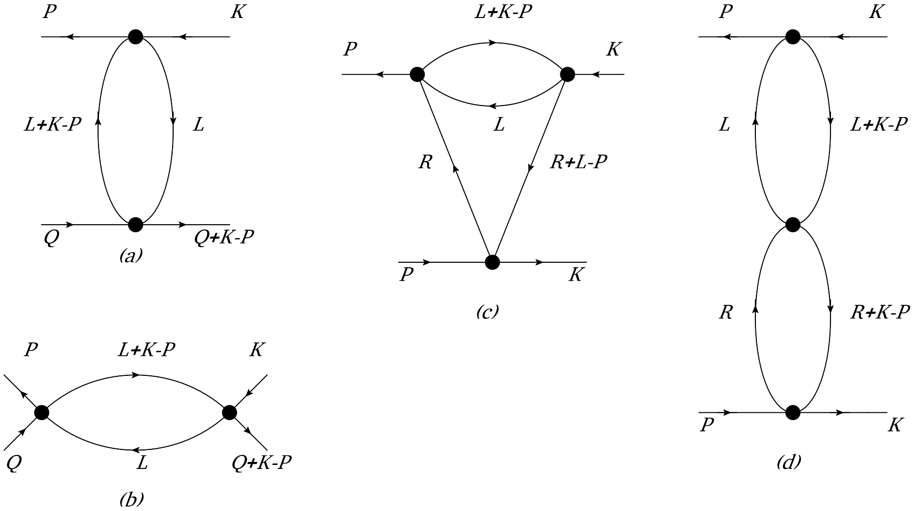

FIG. 2. Some of the loop diagrams that we will study in this paper.

We illustrate the splitting procedure by looking at the 1-loop diagram in part (a). The integral is:

$$I_t^{VV}(-P, Q, K, -Q_t) = \int dL\, V(Q, -Q_t, L, -L_t) G_L G_{L_t} V(-L, L_t, -P, K)\,. \tag{15}$$

We define: $f_1(\{P_i\}, L) = V(Q, -Q_t, L, -L_t) G_L$ and $f_2(\{P_i\}, L) = G_{L_t} V(-L, L_t, -P, K)$ and use (14) to write:

$$I_t^{VV}(-P, Q, K, -Q_t) = \int dL[(\Delta_L f_1 + f_1(0, L))(\Delta_L f_2 + f_2(0, L))]\,. \tag{16}$$

Expanding the square bracket gives four terms. The three terms that contain at least one Δ_L are finite. The remaining term is momentum independent. We have:

$$I_t^{VV}(-P, Q, K, -Q_t) = I_t^{(VV\,\text{fin})}(-P, Q, K, -Q_t) + I_1(V_0, V_0)\,, \tag{17}$$

where we written the momentum independent divergent term:

$$I_1(V_0, V_0) = \int dL\; V(0, 0, L, -L) G_L^2 V(L, -L, 0, 0)\,. \tag{18}$$

Equation (17) is shown schematically in figure 3.

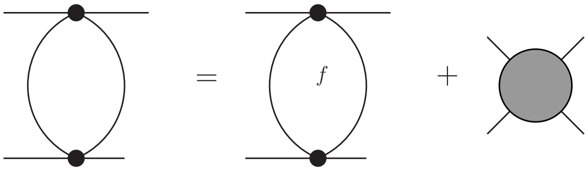

FIG. 3. Diagrammatic representation of equation (17). The grey blob represents the momentum independent divergent integral $I_1(V_0, V_0)$ defined in equation (18).

We will also need to consider 1-loop graphs like the one in part (a) of figure 2 but with one or two bare vertices. The procedure is exactly the same. For example, if the upper vertex is bare, we define $f_1 = \lambda G_L$ and repeat the calculation above. Note that $\Delta_L f_1$ is zero in this case, so there are only two terms in the expansion, one of which is finite, and the other momentum independent. We write the result for one and two bare vertices:

$$I_t^{\lambda V}(-P,Q,K,-Q_t) = I_t^{(\lambda V\,\mathrm{fin})}(-P,Q,K,-Q_t) + I_1(\lambda_0, V_0)\,, \tag{19}$$
$$I_t^{\lambda\lambda}(-P,Q,K,-Q_t) = I_t^{(\lambda\lambda\,\mathrm{fin})}(-P,Q,K,-Q_t) + I_1(\lambda_0, \lambda_0)\,.$$

We can follow the same procedure for the u- and s-channels. For example, the integral for the s-channel diagram in part (b) of figure 2 is:

$$I_s^{VV}(-P,Q,K,-Q_t) = \int dL\, V(Q,-P,L,-L_s) G_L G_{L_s} V(-L,L_s,K,-Q_t,)\,. \tag{20}$$

We define $f_1 = V(Q,-P,L,-L_s)G_L$ and $f_2 = G_{L_s}V(-L,L_s,K,-Q_t)$. Splitting gives:

$$I_s^{VV}(-P,Q,K,-Q_t) = I_s^{(VV\,\mathrm{fin})}(-P,Q,K,-Q_t) + I_1(V_0,V_0)\,. \tag{21}$$

One can follow the same procedure for all 1-loop graphs. The finite contribution depends on the channel, but the momentum independent divergence is the same for all three channels. We write the results as in equations (17) and (19) with a subscript t or u or s on the finite part to indicate the channel.

Now we consider the 2-loop graph in part (c) of figure 2, which we call the triangle graph. The upper loop is $I_s^{VV}(-P,R,K,-R_t)$ (see equation (20)), and thus we have:

$$I_{\mathrm{tri}}(-P,P,K,-K) = \int dR\, I_s^{VV}(-P,R,K,-R_t) G_R G_{R_t} V(-R,R_t,P,-K)\,. \tag{22}$$

Using equation (21) to rewrite $I_s^{VV}(-P,R,K,-R_t)$ as the sum of a finite and divergent piece we obtain:

$$I_{\mathrm{tri}}(-P,P,K,-K) = \int dR\, [I_s^{(VV\,\mathrm{fin})}(-P,R,K,-R_t) + I_1(V_0,V_0)] \cdot (G_R G_{R_t} V(-R,R_t,P,-K))\,. \tag{23}$$

The second term in the square bracket contains an overlapping divergence which we will show can be cancelled by a counter-term. We extract this term:

$$I_{\mathrm{tri}}(-P,P,K,-K)|_{\mathrm{overlap}} =: I_1(V_0,V_0)F(K,P)\,, \tag{24}$$

where we have defined:

$$F(K,P) = \int dL\ \left(G_R G_{R_t} V(-R,R_t,P,-K)\right). \tag{25}$$

Now we look at the first term in the square bracket in equation (23). Defining $f_1(\{P_i\},R) = I_s^{(VV\,\text{fin})}(-P,R,K,-R_t)$ and $f_2(\{P_i\},R) = G_R G_{R_t} V(-R,R_t,P,-K)$ and using (14) we get four terms. The three terms that contain at least one Δ_R are finite. The remaining term is a momentum independent divergence:

$$\begin{aligned} I_{\text{tri}}(-P,P,K,-K)\big|_{\text{divergence}} &= \int dR\, I_s^{(VV\,\text{fin})}(0,R,0,-R)G^2(R)V(-R,R,0,0)\,, \\ &=: I_3(V_0,\text{bub}_{f0})\,, \end{aligned} \tag{26}$$

where the notation bub_{f0} indicates the finite part of the bubble insertion in the s-channel. Combining the results in (24) and (26) we have:

$$I_{\text{tri}}(-P,P,K,-K)\ =\ \text{finite}\ +\ I_1(V_0,V_0)F(K,P) + I_3(V_0,\text{bub}_{f0})\,. \tag{27}$$

This result is shown schematically in figure 4.

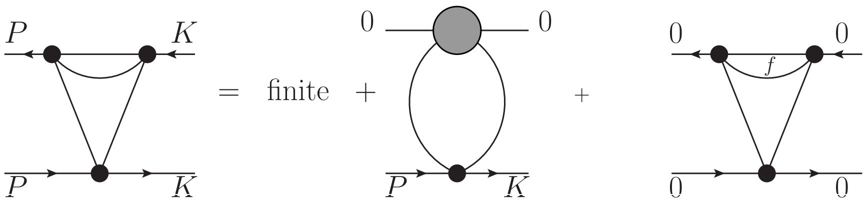

FIG. 4. Diagrammatic representation of equation (27).

Now we look at the 2-loop diagram in part (d) of figure 2 which we call the double-scoop diagram. This diagram is a little harder to handle because of the internal vertex which does not connect with any external legs. The upper loop is $I_t^{VV}(-P,K,R,-R_t)$ (see equation (15)), and thus we have:

$$I_{\text{dsc}}(-P,P,K,-K) = \int dR\, I_t^{VV}(-P,K,R,-R_t)G_R G_{R_t} V(-R,R_t,P,-K)\,. \tag{28}$$

We rewrite the t-loop insertion by doing the same calculation that allowed us to rewrite (15) as (17). However, the t-loop insertion in (28) has external legs that connect to the lower loop, and thus they carry momenta that are not external to the diagram as a whole. In order to deal with this vertex, we split it in external variables only:

$$V(L_t,-L,-R_t,R) = [V(L_t,-L,-R_t,R) - V(L,-L,-R,R)] + V(L,-L,-R,R)\,. \tag{29}$$

This splitting is advantageous because the quantity in square brackets is $\sim 1/L$ when L is large, and $\sim 1/R$ when R is large, and therefore acts like either Δ_L or Δ_R, depending on which integral is under consideration. Using this strategy, it is straightforward to see that equations (17) and (18) are modified to become:

$$I_t^{VV}(-P,K,R,-R_t) = I_t^{VV\,\text{fin}}(-P,K,R,-R_t) + \int dL\ V(0,0,L,-L)G_L^2 V(L,-L,-R,R)\,. \tag{30}$$

In addition, we split the second factor in (28) using (14) with $f_1(\{P_i\}, R) = G_R G_{R_t} V(-R, R_t, P, -K)$. Combining we have:

$$\begin{aligned} &I_{\rm dsc}(-P,P,K,-K) \\ &\quad = \int dR\, \left[I_t^{VV\,{\rm fin}}(-P,K,R,-R_t) + \int dL\, V(0,0,L,-L) G_L^2 V(L,-L,-R,R) \right] \cdot \left[\Delta_R f_1 + f_1(0,R) \right] . \end{aligned} \tag{31}$$

Expanding we get four terms. Taking the first term in each square bracket gives:

$$\text{term}_1 = \int dR\, I_t^{VV\,{\rm fin}}(-P,K,R,-R_t)\, \Delta_R f_1 \quad = \quad \text{finite} . \tag{32}$$

Taking the last term in each square bracket gives a momentum independent divergence:

$$\text{term}_2 = \int dR \int dL\, V(0,0,L,-L) G_L^2 V(L,-L,-R,R) G_R^2 V(-R,R,0,0) =: I_2(V_0, V, V_0) . \tag{33}$$

The first cross-term in (31) is:

$$\text{cross}_1 = \int dR \, \int dL\, V(0,0,L,-L) G_L^2 V(L,-L,-R,R) \Delta_R f_1 . \tag{34}$$

The integral over R is finite, but the integral over L is not. We divide the L integral into a finite and divergent piece by splitting the middle vertex. Choosing $f_2(\{P_i\}, L) = V(L,-L,-R,R)$ and using equation (14) we obtain a term containing a Δ_L which gives a finite result when the L integral is done, and a momentum independent divergence. The result can be written:

$$\begin{aligned} \text{cross}_1 = \text{finite} \; + \; & \int dR \, \int dL\, V(0,0,L,-L) G_L^2 V(L,-L,0,0) \Delta_R f_1 , \\ &= I_1(V_0,V_0) \int dR\, \left(G_R G_{R_t} V(-R,R_t,P,-K) - G_R^2 V(-R,R,0,0) \right) , \\ &= I_1(V_0,V_0) F(K,P) - I_1(V_0,V_0) \frac{1}{\lambda} I_1(\lambda, V_0) , \end{aligned} \tag{35}$$

where we expanded $\Delta_R f_1$ in the second line, and used (18) and (25) in the last line.

The second cross-term in (31) is:

$$\begin{aligned} \text{cross}_2 = & \int dR\, I_t^{VV\,{\rm fin}}(-P,K,R,-R_t)\, f_1(0,R) , \\ = & \int dR \int dL [V(-P,K,L,-L_t) G_{L_t} G_L V(-L,L_t,R,-R_t) - V(0,,0,L,-L) G_L^2 V(-L,L,R,-R)] \\ & \quad \cdot\, G_R^2 V(R,-R,0,0) , \end{aligned} \tag{36}$$

where we used (30) to expand the insertion $I_t^{VV\,{\rm fin}}$. The integration over L is finite, but the integration over R is not. We split both of the middle vertices to construct a Δ_R by choosing $f_3(\{P_i\}, R) = V(-L, L_t, R, -R_t)$ and $f_4(\{P_i\}, R) = V(-L, L, R, -R)$. The sum of the two Δ_R terms is finite. We obtain:

$$\begin{aligned} &\text{cross}_2 = \text{finite} \\ &\quad + \int dL \int dR [V(-P,K,L,-L_t) G_{L_t} G_L V(0,0,R,-R) - V(0,0,L,-L) G_L^2 V(0,0,R,-R)] \\ &\qquad \cdot\, G_R^2 V(R,-R,0,0) , \\ &\quad = \text{finite} + F(-K,-P) I_1(V_0,V_0) - \frac{1}{\lambda} I_1(\lambda, V_0) I_1(V_0,V_0) , \end{aligned} \tag{37}$$

where we used (18) and (25) in the last line. The full result for the double-scoop diagram is obtained by combining equations (32), (33), (35) and (37). In many equations and figures in this paper we do not include separately contributions that correspond to different permutations of the external legs, but use numerical factors in brackets to indicate the presence of terms or diagrams that correspond to permutations which are not written explicitly. Using this notation we write $F(K,P)+F(-K,-P)=(2)F(K,P)$ and the full result for the double-scoop diagram is:

$$I_{\rm dsc}(-P,P,K,-K)=\text{finite}\ +\ (2)F(K,P)I_1(V_0,V_0)-2\frac{1}{\lambda}I_1(\lambda,V_0)I_1(V_0,V_0)+I_2(V_0,V,V_0)\,. \tag{38}$$

This result is shown schematically in figure 5. The factors (2) in the diagrams indicate that the graphs with the grey blob on the lower vertex are also included.

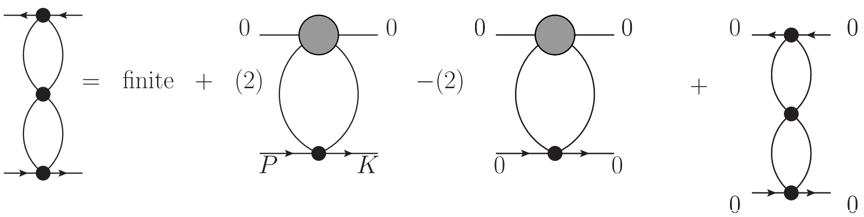

FIG. 5. Diagrammatic representation of equation (38).

V. RENORMALIZATION OF THE 4-POINT FUNCTION

The equation of motion for the 4-point function is obtained from the variational equation $\delta\Gamma/\delta V=0$. From this point onward, we suppress the last momentum argument in the 4-point function V, since it can be obtained from the conservation of momentum. The effective action in figure 1 gives:

$$V(P_a,P_b,P_c)=\lambda+\delta\lambda_{bb}+V_s(P_a,P_b,P_c)+V_t(P_a,P_b,P_c)+V_u(P_a,P_b,P_c)\,, \tag{39}$$

with

$$\begin{aligned} V_s(P_a,P_b,P_c) &\equiv \frac{1}{2}\int dQ\; V(P_a,P_c,Q)G(Q)G(Q+P_a+P_c)V(P_b,P_d,-Q)\,, \\ V_t(P_a,P_b,P_c) &= V_s(P_a,P_c,P_b)\,, \\ V_u(P_a,P_b,P_c) &= V_s(P_a,P_b,P_d)\,, \end{aligned} \tag{40}$$

where $P_d=-(P_a+P_b+P_c)$. The corresponding diagrams are shown in figure 6.

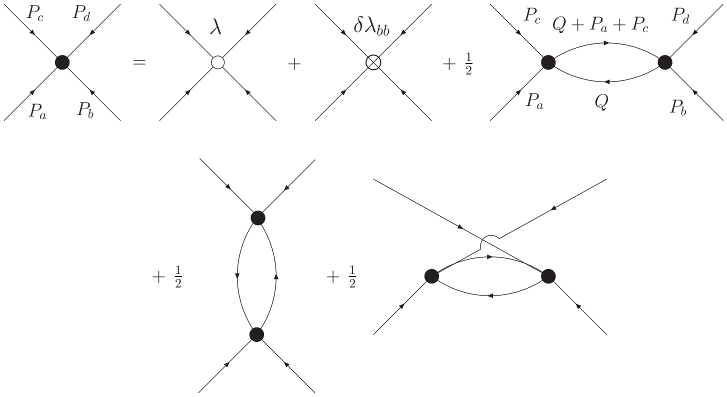

FIG. 6. Self-consistent equation of motion for the proper 4-point vertex.

Combining permutations of external legs, the diagrams in figure 6 are represented as in figure 7. The factor (3) indicates that there are 3 channels, only one of which is drawn.

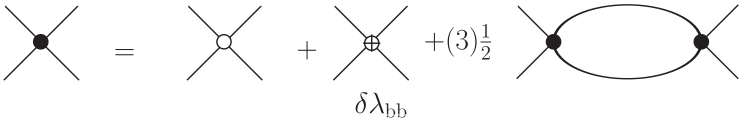

FIG. 7. The equation of motion in figure 6 with only one channel drawn explicitly.

From equations (17) and (21) it is clear that all three channels will produce the same divergent contribution. Using the result in equation (17) and figure 3, the vertex is renormalized by a 1-loop counter-term:

$$\delta\lambda^{(1)}_{\rm bb} = -\frac{3}{2} I_1(V_0, V_0)\,. \tag{41}$$

VI. RENORMALIZATION OF THE 2-POINT FUNCTION

In this section we discuss the renormalization of the 2-point function. In section VI A we show that the 2-point function can be written in terms of another 4-point vertex which we will call M. In section VI B we prove that this 4-point function can be renormalized with an appropriate choice of the counter-term $\delta\lambda_{\rm et}$. In section VII we will show this counter-term is the same as the counter-term $\delta\lambda_{\rm bb}$ which was used to renormalize the 4-point function in section V, to within the approximation order of the theory.

A. Definition of the Bethe-Salpeter vertex

We show below that the divergent terms in the 2-point function can be packaged into a 4-point vertex. The discussion in this section follows exactly that of reference [19] and is included only for completeness. The self-energy is defined through the Dyson equation and the equation of motion for the 2-point function:

$$G^{-1} = G_0^{-1} - \Sigma\,, \quad \Sigma = 2\frac{\delta\Phi_{\rm int}}{\delta G}\,. \tag{42}$$

Including all momentum variables, the expression for the self-energy is:

$$\Sigma(p) = i(\delta Z P^2 - \delta m^2) + \frac{1}{2}(\lambda + \delta\lambda_{\rm et}) \int dQ\; G(Q)$$
$$+\frac{1}{6}(\lambda + \delta\lambda_{\rm bb}) \int dQ \int dK\; V(P,Q,K)G(Q)G(K)G(Q+K+P). \tag{43}$$

In order to extract the leading asymptotic behaviour we define:

$$\tilde{G} = G_{\rm as} + \delta G\,, \quad \Sigma(\tilde{G}) = \Sigma_{\rm as} + \Sigma_0\,, \tag{44}$$

where $G_{\rm as} \sim P^{-2}$ and $\Sigma_{\rm as} \sim P^2$ contain the leading asymptotic behaviour of the propagator and self-energy respectively. From (42) (and using the bare propagator defined in (2)) we obtain:

$$\tilde{G} = G_{\rm as} + G_{\rm as}^2(-im^2 + \Sigma_0) + \cdots \quad \to \quad \delta G = G_{\rm as}^2(-im^2 + \Sigma_0) + \cdots\,. \tag{45}$$

We define two new 4-point vertices: a kernel Λ, and a vertex M obtained from Λ by solving a self-consistent integral equation. Both of these vertices will only be needed with momentum arguments $(P,-P,K,-K)$ and we will use the short hand notation $\Lambda(P,-P,K,-K) = \Lambda(P,K)$ and $M(P,-P,K,-K) = M(P,K)$. We define:

$$\Lambda(P,K) = 4\frac{\delta^2\Phi_{\rm int}[G,V]}{\delta G(P)G(K)}\,, \tag{46}$$

$$M(P,K) = \Lambda(P,K) + \frac{1}{2}\int dR\,\Lambda(P,R)G(R)^2 M(R,K)\,. \tag{47}$$

From equations (44) and (46) we obtain:

$$\Sigma_{\rm as} + \Sigma_0 = \Sigma[G_{\rm as} + \delta G]\,, \tag{48}$$
$$\to \quad \Sigma_0(K) = -i\delta m^2 + \frac{1}{2}\int dP\delta G(P)\Lambda_{\rm as}(P,K) + \text{ finite terms}\,,$$
$$= -i\delta m^2 + \frac{1}{2}\int dP\delta G(P)\Lambda_{\rm as}(P,0) + \text{ finite terms}\,.$$

To obtain the second line we expanded $\Sigma[G_{\rm as}+\delta G]$ in δG. In the third line we use the same strategy as in section V: we write $\Lambda_{\rm as}(P,K) = [\Lambda_{\rm as}(P,K) - \Lambda_{\rm as}(P,0)] + \Lambda_{\rm as}(P,0)$, and use Weinberg's theorem to show that the square bracket produces a finite integral.

Next we observe that equation (47) gives:

$$\Lambda_{\rm as}(P,0) = M(P,0) - \frac{1}{2}\int dR\,\Lambda_{\rm as}(P,R)G_{\rm as}^2(R)M(R,0)\,, \tag{49}$$

and substituting (49) into equation (48) gives:

$$\Sigma_0(K) = -i\delta m^2 \tag{50}$$
$$+\frac{1}{2}\int dP[\delta G(P)]M(P,0) - \frac{1}{2}\int dR\Big[\frac{1}{2}\int dP\delta G(P)\Lambda_{\rm as}(P,R)\Big]G_{\rm as}^2(R)M(R,0) + \text{ finite terms}\,.$$

Using (45) and (48) to replace the two square brackets in (50) we have:

$$\Sigma_0(K) = -i\delta m^2 + \text{ finite terms} \tag{51}$$
$$+\frac{1}{2}\int dP[(-im^2 + \Sigma_0(P))G_{\rm as}^2(P)]M(P,0) - \frac{1}{2}\int dR\Big[\Sigma_0(R) + i\delta m^2\Big]G_{\rm as}^2(R)M(R,0)\,.$$

The key point is that the terms involving Σ_0 on the right side cancel. We are left with:

$$\Sigma_0(K) = -i\delta m^2 - \frac{i}{2}(m^2 + \delta m^2)\int dP G_{\rm as}^2(P)M(P,0) + \text{ finite terms}\,. \tag{52}$$

The P-integral is divergent but momentum independent, and can be cancelled by an appropriate choice of the counter-term δm^2. Thus we must show that the vertex M can be renormalized.

B. Renormalization of the vertex M

In this section we discuss the renormalization of the vertex M defined in equation (47). This equation is represented diagrammatically in figure 8.

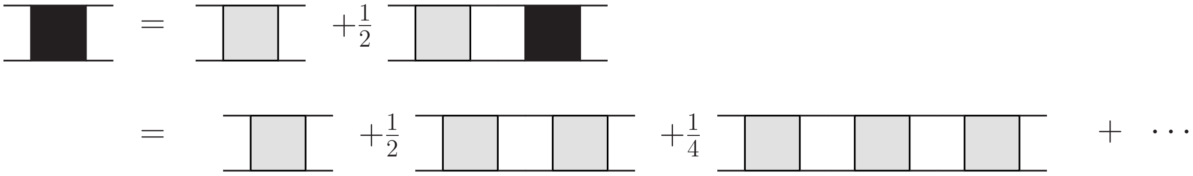

FIG. 8. Diagrammatic representation of equation (47). The black box is the vertex M and the light grey box is the vertex Λ.

We will define $M^{(x)}$ to mean all terms produced by iterating x times, and $m^{(x)}$=$M^{(x)}$-$M^{(x-1)}$ means terms produced at the x-th interation which were not present at the (x-1)-th iteration.

The vertex Λ is obtained from equations (11) and (46) and shown in figure 9. It contains only t- and u-channels. The t-channel is drawn, and the factors (2) indicate that the u-channel is included although it is not drawn. Diagrams that are not symmetric when inverted top to bottom carry a factor (4) to indicate that there are actually four permutations, only one of which is drawn.

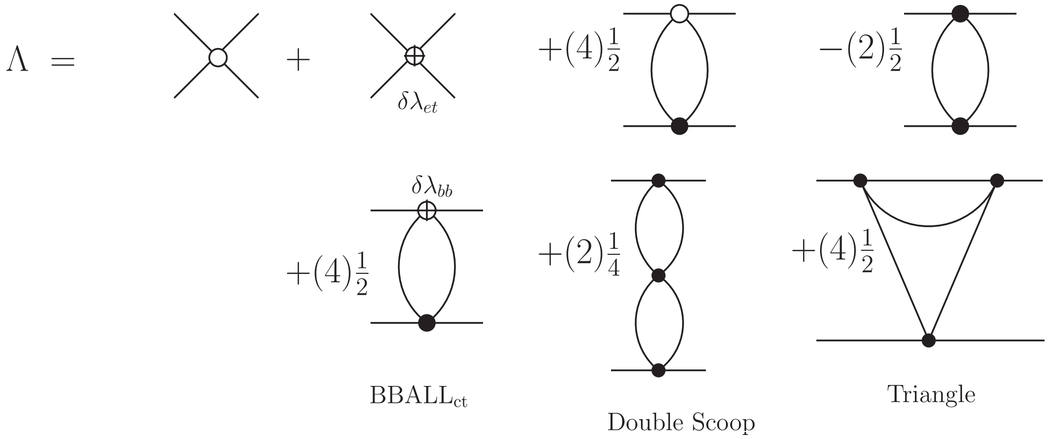

FIG. 9. The kernel Λ.

Consider for the moment the 1-loop contributions to $M^{(1)} = m^{(0)} + m^{(1)}$. The t- and u-channels appear in $m^{(0)} = \Lambda$. The s-channel is the part of $m^{(1)}$ which is produced by the 0-loop piece of Λ:

$$m^{(1)} = \frac{1}{2}\int dL\Lambda(P,L)G^2(L)\Lambda(L,K) = \int dL\lambda G^2(L)\lambda + \cdots\,. \tag{53}$$

Combining these pieces gives the result is shown in figure 10.

$M^{(1)} = m^{(0)} + m^{(1)} = (4)\frac{1}{2}$ 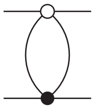 $-(2)\frac{1}{2}$ 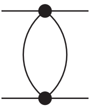 $+\frac{1}{2}$ 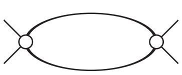

FIG. 10. 1-loop contributions to the vertex M.

Thus we find that $M^{(1)}$ contains 1-loop diagrams which correspond to all three channels, but the t- and u-channels are produced at the level of 0-iterations (in the kernel), and the s-channel does not appear until the first iteration. It is clear that this structure also holds at the 2-loop level: t- and u-channels are contained in the kernel and s-channels are produced by iteration.

In order to show how renormalization works, we divide the counter-terms into pieces and group each piece together with the divergence it cancels. To do this, we introduce a parameter c which serves as a counter so that all terms in $m^{(x)}$ are proportional to c^x. The parameters c is introduced only for organizational convenience and will be set to one at the end of the day. Using this notation we write the counter-term in the Lagrangian:

$$\delta\lambda_{\rm et} = \delta\lambda_{\rm et}^{\rm bp} + \Delta\lambda_{\rm et}\,, \quad \Delta\lambda_{\rm et} = \sum_i c^i \Delta\lambda_{\rm et}^{({\rm it}\,i)}\,, \tag{54}$$

where the notation $\Delta\lambda_{\rm et}^{({\rm it}\,i)}$ indicates the contribution to the counter-term $\Delta\lambda$ produced by the ith iteration. The factor c in the expansion of $\Delta\lambda_{\rm et}$ ensures that contributions from this counter-term are grouped not with terms from the kernel, but with terms that are produced by iteration. This grouping allows us to show that all overlapping divergences cancel, and to construct the counter-term that cancels the remaining overall divergence.

As a first step, we substitute equation (54) into the expression for the vertex Λ and write the result:

$$\Lambda = \Lambda[\delta\lambda_{\rm et}^{\rm bp}, \delta\lambda_{\rm bb}] + \Delta\lambda_{\rm et} =: \Lambda_f + \Delta\lambda_{\rm et}\,. \tag{55}$$

The notation $\Lambda[\delta\lambda_{\rm et}^{\rm bp}, \delta\lambda_{\rm bb}]$ means the vertex in figure 9 with the full counter-term $\delta\lambda_{\rm et}$ replaced by only the piece $\delta\lambda_{\rm et}^{\rm bp}$. The counter-terms $\delta\lambda_{\rm et}^{\rm bp}$ and $\delta\lambda_{\rm bb}$ are chosen to make Λ finite, and this finite piece is denoted Λ_f. These counter-terms can be obtained from figure 9, using the results in equations (17), (27) and (38) (see figures 3, 4 and 5). We obtain:

$$\delta\lambda_{\rm et}^{{\rm bp}\,(1)} = -(4)\frac{1}{2}I_1(\lambda, V_0) + (2)\frac{1}{2}I_1(V_0, V_0)\,, \tag{56}$$

$$\delta\lambda_{\rm bb}^{(1)} = -\frac{3}{2}I_1(V_0, V_0)\,, \tag{57}$$

$$\delta\lambda_{\rm et}^{{\rm bp}\,(2)} = -(2)\frac{1}{4}\Big[I_2(V_0, V, V_0) - 2\frac{1}{\lambda}I_1(\lambda, V_0)I_1(V_0, V_0)\Big] - (4)\frac{1}{2}I_3(V_0, {\rm bub}_{f0})\,, \tag{58}$$

where the super-scripts indicate the loop order of each contribution. Note that equations (41) and (57) agree.

Now we look at the vertex M. We rewrite equation (47) with a factor c inserted to keep track of the iteration order:

$$M(P,K) = \Big[\Lambda_f(P,K) + \Delta\lambda_{\rm et}\Big] + \frac{1}{2}\,c\int dR\,\Big[\Lambda_f(P,R) + \Delta\lambda_{\rm et}\Big]G(R)^2 M(R,K)\,. \tag{59}$$

We show below that this equation can be renormalized using $\Delta\lambda_{\rm et}$ self-consistently determined from the equation:

$$\Delta\lambda_{\rm et} = -\frac{1}{2}c\int dL\,[\Lambda_f(0,L) + c\,\Delta\lambda_{\rm et}]\,G^2(L)M(L,0)\,. \tag{60}$$

Since both equations (59) and (60) involve only the s-channel, we can suppress all momentum arguments without ambiguity if we maintain the order of the factors in every term. Using this notation equations (59) and (60) become:

$$M = \Big[\Lambda_f + \Delta\lambda_{\rm et}\Big] + \frac{1}{2}\,c\,\Big[\Lambda_f + \Delta\lambda_{\rm et}\Big]G^2 M\,, \tag{61}$$

$$\Delta\lambda_{\rm et} = -\frac{1}{2}c\,[(\Lambda_f + c\,\Delta\lambda_{\rm et})G^2 M]_{00}\,, \tag{62}$$

where the subscript 00 in the second line indicates that the legs on both sides of the diagram carry zero momentum.

Now we substitute $\Delta\lambda_{\rm et} = \sum_i c^2\Delta\lambda_{\rm et}^{({\rm it}\,i)}$ (see equation (54)) and collect powers of c. At order c^0 we obtain:

$$c^0:\quad \Delta\lambda^{({\rm it}\,0)} = 0\,,\qquad M^{(0)} = m^{(0)} = \Lambda_f\,. \tag{63}$$

At order c^1 we have:

$$\begin{aligned} c^1:\quad \Delta\lambda_{\rm et}^{({\rm it}\,1)} &= -\frac{1}{2}[\Lambda_f G^2 m^{(0)}]_{00} = -\frac{1}{2}[\Lambda_f G^2\Lambda_f]_{00} = -\frac{1}{2}I_1(\Lambda_{f0},\Lambda_{f0})\,,\\ m^{(1)} &= \Delta\lambda_{\rm et}^{({\rm it}\,1)} + \frac{1}{2}\Lambda_f G^2 m^{(0)} = \Delta\lambda_{\rm et}^{({\rm it}\,1)} + \frac{1}{2}\Lambda_f G^2\Lambda_f\,, \end{aligned} \tag{64}$$

where in the first line we have used the same notation as in equation (18) with the proper 4-vertex replaced by the vertex Λ_f. To see that $m^{(1)}$ is finite, we split the vertex Λ_f using the same method as in section IV. We introduce a diagrammatic notation which is shown in figure 11.

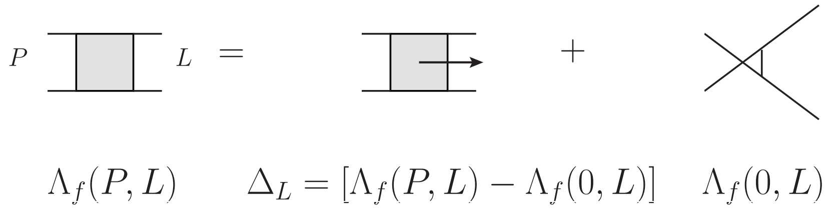

FIG. 11. Splitting the kernel Λ_f. The arrow on the grey box indicates that the vertex has been split to the right. The integral over the loop connected to the legs on the right side of the box will be finite.

We define a general procedure for splitting s-channel graphs of the form shown in figure 8 at any order in c. In all graphs, start from the right-most Λ_f vertex and split it towards the left. If the loop to the left of this vertex is made finite by the splitting then split the next vertex left, if the loop to the left of the original vertex is not finite, then split the next vertex right. Continue moving across the diagram towards the left until reaching the left-most vertex. Split this vertex to the right. The application of this procedure to the vertex $m^{(1)}$ (see equation (64)) is shown in figure 12.

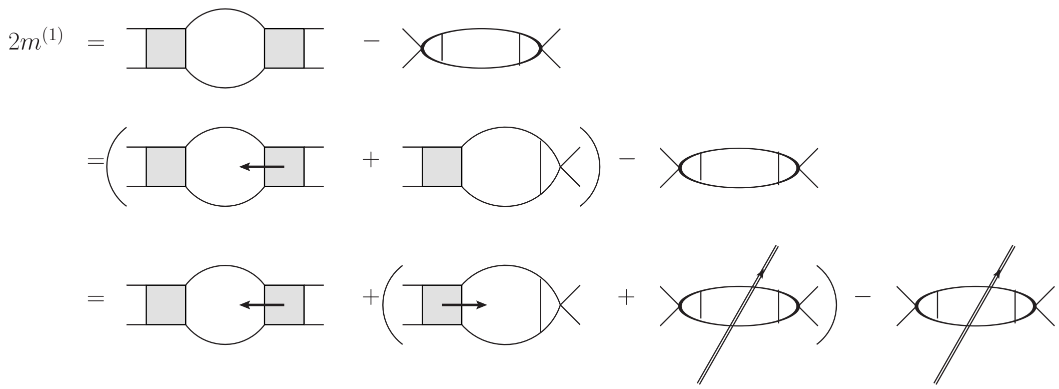

FIG. 12. Splitting the first iteration of M. The divergent piece cancels.

Now we look at terms of order c^2. The counter-term (from equation (62)) is:

$$\Delta\lambda_{\rm et}^{(\rm it\,2)} = -\frac{1}{2}[\Delta\lambda_{\rm et}^{(\rm it\,1)} G^2 \Lambda_f]_{00} - \frac{1}{2}[\Lambda_f G^2 m^{(1)}]_{00}\,. \tag{65}$$

We substitute $m^{(1)}$ and $\Delta\lambda^{(\rm it\,1)}$ from the previous step. Note that the first diagram in the last line of figure 12 drops out because the split vertex on the right end has the form $\Delta_L = \Lambda_f(L,K) - \Lambda_f(L,0)$ and gives identically zero when we set the external momentum to zero. In the second diagram we re-expand the split vertex and write the full result as:

$$\Delta\lambda_{\rm et}^{(\rm it\,2)} = \frac{1}{2} I_1(\Lambda_{f0},\Lambda_{f0})\frac{1}{\lambda} I_1(\lambda,\Lambda_{f0}) - \frac{1}{4} I_2(\Lambda_{f0},\Lambda_f,\Lambda_{f0})\,, \tag{66}$$

where we have used equation (64) and the same notation as in equations (18) and (33) with the proper 4-vertex replaced by the vertex Λ_f. Equation (66) is shown in figure 13.

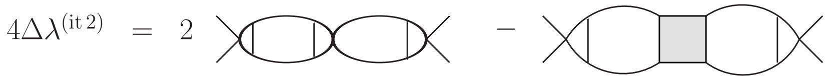

FIG. 13. Diagrammatic representation of the counter-term $\Delta\lambda^{(\rm it\,2)}$ in equation (65).

The vertex $m^{(2)}$ (from equation (61)) is:

$$m^{(2)} = \frac{1}{2}\Delta\lambda_{\rm et}^{(\rm it\,1)} G^2 \Lambda_f + \frac{1}{2}\Lambda_f G^2 m^{(1)} + \Delta\lambda_{\rm et}^{(\rm it\,2)}\,. \tag{67}$$

The graphs obtained by substituting the results for $\Delta\lambda_{\rm et}^{(\rm it\,1)}$, $m^{(1)}$ and $\Delta\lambda_{\rm et}^{(\rm it\,2)}$ from previous steps are shown on the left side of figure 14. The results of the vertex splitting procedure are shown on the right. Terms that cancel are marked in pairs with the letters (x), (y), (z), (u) and (v). The remaining terms are finite.

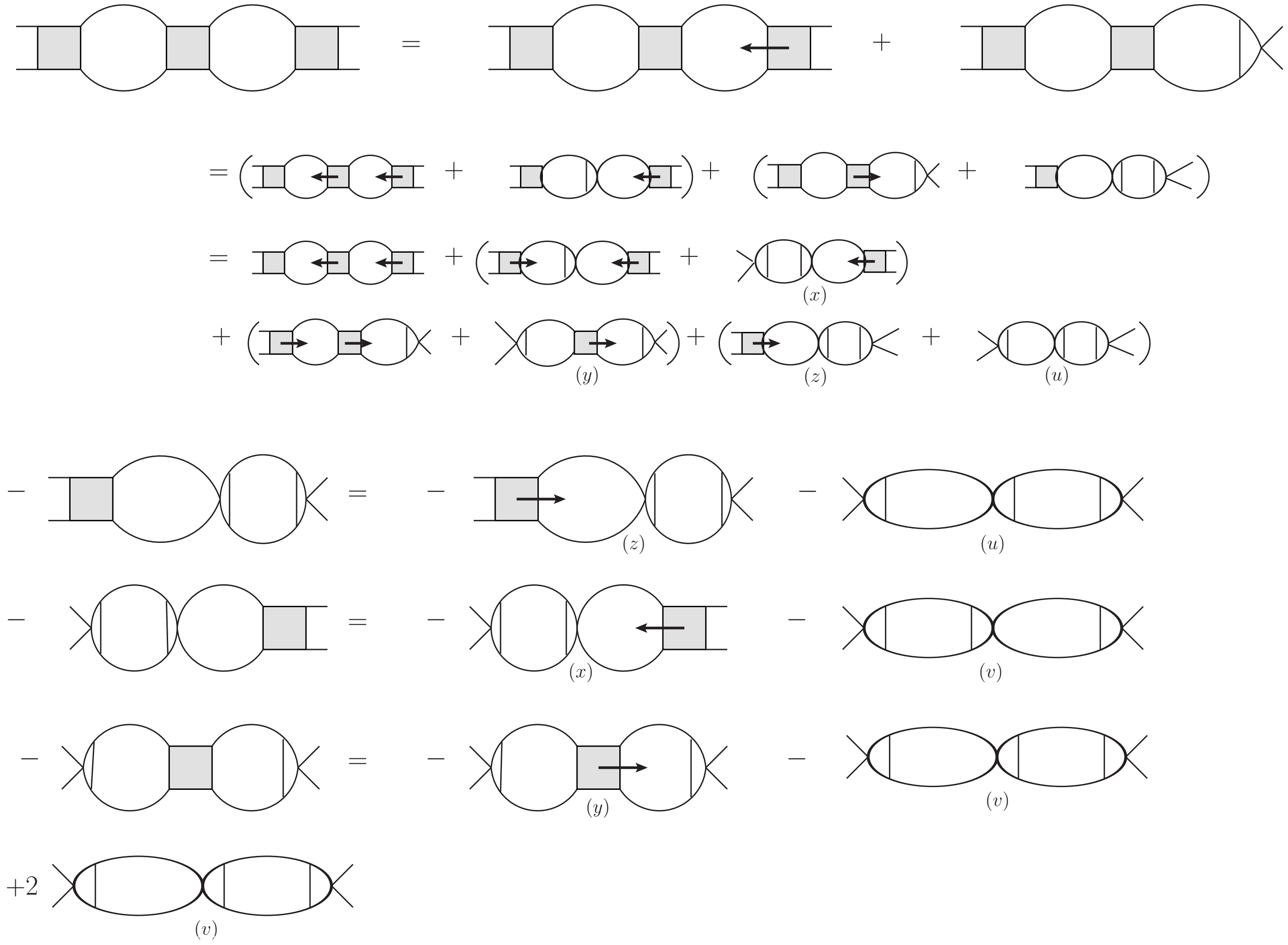

FIG. 14. Splitting $4m^{(2)}$ towards the left.

It is straightforward to see how to apply this procedure at an arbitrary number of iterations. Each iteration produces one diagram of the form $\Lambda_f G^2 \Lambda_f G^2 \Lambda_f G^2 \cdots \Lambda_f$ which contains a series of overlapping divergences that have the form of the terms on the right side of the first line in figure 14. The counter-term obtained from (60) contains exactly the right series of nested insertions to remove these overlapping divergences.

VII. EQUIVALENCE OF THE COUNTER-TERMS

A. Renormalization of the vertex M to 2-Loops in the skeleton expansion

In this section we study the renormalization of M to 2-loops in the skeleton expansion. In the next section we will show that the counter-terms that make M finite at 2-Loops are the same as those that make the proper vertex V finite when it's calculated from the equation of motion to 2-loops in the skeleton expansion.

For convenience we collect all pieces of the counter-term $\delta\lambda_{\rm et}$ which are produced by the first two iterations (see equations (56), (58), (64) and (66)):

$$\begin{aligned}
\delta\lambda_{\rm et} &= \delta\lambda_{\rm et}^{\rm bp\,(1)} + \delta\lambda_{\rm et}^{\rm bp\,(2)} + \Delta\lambda_{\rm et}^{\rm (it\,1)} + \Delta\lambda_{\rm et}^{\rm (it\,2)} \; + \; \cdots\,, \\
\delta\lambda_{\rm et}^{\rm bp\,(1)} &= -(4)\frac{1}{2}I_1(\lambda,V_0) + (2)\frac{1}{2}I_1(V_0,V_0)\,, \qquad (68)\\
\delta\lambda_{\rm et}^{\rm bp\,(2)} &= -(2)\frac{1}{4}\Big[I_2(V_0,V,V_0) - 2\frac{1}{\lambda}I_1(\lambda,V_0)I_1(V_0,V_0)\Big] - (4)\frac{1}{2}I_3(V_0,{\rm bub}_{f0})\,, \qquad (69)\\
\Delta\lambda_{\rm et}^{\rm (it\,1)} &= -\frac{1}{2}I_1(\Lambda_{f0},\Lambda_{f0})\,, \qquad (70)\\
\Delta\lambda_{\rm et}^{\rm (it\,2)} &= -\frac{1}{4}\Big[I_2(\Lambda_{f0},\Lambda_f,\Lambda_{f0}) - 2I_1(\Lambda_{f0},\Lambda_{f0})\frac{1}{\lambda}I_1(\lambda,\Lambda_{f0})\Big]\,. \qquad (71)
\end{aligned}$$

Recall that $\delta\lambda_{\rm et}^{(1)}$ and $\delta\lambda_{\rm et}^{(2)}$ are the 1- and 2-loop counter-terms that renormalize the kernel Λ, and $\Delta\lambda_{\rm et}^{\rm (it\,1)}$ and $\Delta\lambda_{\rm et}^{\rm (it\,2)}$ are the counter-terms that renormalize M to 1- and 2-iterations. Since the vertex Λ_f contains 2-loop terms, we need to separate the 1- and 2-loop pieces of $\Delta\lambda_{\rm et}^{\rm (it\,1)}$. We write:

$$\begin{aligned}
\Delta\lambda_{\rm et}^{\rm (it\,1)} &= \Delta\lambda_{\rm et}^{\rm (it\,1)}\Big|_{\rm 1\,loop} + \Delta\lambda_{\rm et}^{\rm (it\,1)}\Big|_{\rm 2\,loop}\,, \qquad (72)\\
\Delta\lambda_{\rm et}^{\rm (it\,1)}\Big|_{\rm 1\,loop} &= -\frac{1}{2}[\Lambda_f^{(0)}G^2(L)\Lambda_f^{(0)}]_{00} = -\frac{1}{2}I_1(\lambda,\lambda)\,, \qquad (73)\\
\Delta\lambda_{\rm et}^{\rm (it\,1)}\Big|_{\rm 2\,loop} &= -\frac{1}{2}(2)[\Lambda_f^{(0)}G^2(L)\Lambda_f^{(1)}]_{00}\,, \qquad (74)
\end{aligned}$$

where $\Lambda_f^{(0)}$ and $\Lambda_f^{(1)}$ are the 0- and 1-loop parts of the finite kernel.

The 1-loop counter-term is obtained from equations (68) and (73):

$$\delta\lambda_{\rm et}^{(1)} = \delta\lambda_{\rm et}^{\rm bp\,(1)} + \Delta\lambda_{\rm et}^{\rm (it\,1)}\Big|_{\rm 1\,loop} = -(4)\frac{1}{2}I_1(\lambda,V_0) + (2)\frac{1}{2}I_1(V_0,V_0) - \frac{1}{2}I_1(\lambda,\lambda)\,. \qquad (75)$$

Equation (75) is shown in figure 15.

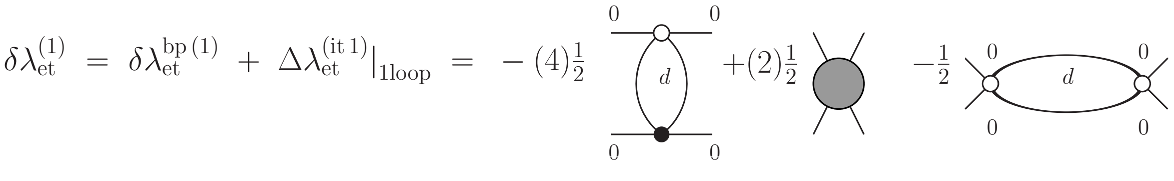

$\delta\lambda_{\rm et}^{(1)} \;=\; \delta\lambda_{\rm et}^{\rm bp\,(1)} \;+\; \Delta\lambda_{\rm et}^{\rm (it\,1)}|_{\rm 1loop} \;=\; -\,(4)\frac{1}{2}$
0
0
d
0
0
$+(2)\frac{1}{2}$
$-\frac{1}{2}$
0
0
d
0
0

FIG. 15. Diagrammatic representation of the 1-loop counter-term in equation (75).

Now we look at the 2-loop terms. At 2-loop order in the skeleton expansion we can rewrite the 2-loop contribution to $\Delta\lambda_{\rm et}^{\rm (it\,1)}$ in equation (74) using $\Lambda_f^{(0)} = \lambda \to V$ and $\Lambda_f^{(1)}(\lambda,V) \to \Lambda_f^{(1)}(V,V)$ where $\Lambda_f^{(1)}(V,V)$ is the two 1-loop graphs in figure 9 with the bare vertex λ replaced by the proper vertex V. The result is shown in figure 16.

$$\Delta\lambda_{\rm et}^{(\rm it\,1)}\big|_{2\,\rm loop} \;=\; -\,(2)\tfrac{1}{2}$$

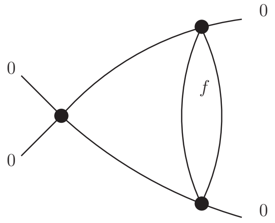

$$=\; -\,I_3(V_0, {\rm bub}_{f0})$$

FIG. 16. 2-loop contribution from $\Delta\lambda_{\rm et}^{(\rm it\,1)}$.

Similarly we can rewrite the result for $\Delta\lambda_{\rm et}^{(\rm it\,2)}$ in equation (71) by replacing $\Lambda_f \to \Lambda_f^{(0)} = \lambda \to V$. The result is:

$$\Delta\lambda_{\rm et}^{(\rm it\,2)}\bigg|_{2\,\rm loop} = -\frac{1}{4}\Big[I_2(V_0,V,V_0) - 2\frac{1}{\lambda}I_1(\lambda,V_0)I_1(V_0,V_0)\Big]\,. \tag{76}$$

Combining the 2-loop contributions in equations (74) and (76) (see figure 16) and comparing with equation (69) we have:

$$\Delta\lambda_{\rm et}^{(2)} = \Delta\lambda_{\rm et}^{(\rm it\,2)}\bigg|_{1\,\rm loop} + \Delta\lambda_{\rm et}^{(\rm it\,2)}\bigg|_{2\,\rm loop} = \frac{1}{2}\delta\lambda_{\rm et}^{\rm bp\,(2)}\,. \tag{77}$$

From equations (69) and (77) the full 2-loop counter-term is:

$$\begin{aligned}\delta\lambda_{\rm et}^{(2)} &= \delta\lambda_{\rm et}^{\rm bp\,(2)} + \Delta\lambda_{\rm et}^{(2)}\,, \\ &= -(3)\Big\{\frac{1}{4}\Big[I_2(V_0,V,V_0) - 2\frac{1}{\lambda}I_1(\lambda,V_0)I_1(V_0,V_0)\Big] \;+\; (2)\frac{1}{2}I_3(V_0,{\rm bub}_{f0})\Big\}\,.\end{aligned} \tag{78}$$

B. Renormalization of the vertex V to 2-Loops in the skeleton expansion

In this section we show that the vertices $V(-P,P,K,-K)$ and $M(-P,P,K,-K)$ are renormalized by the same counter-terms, to within the truncation order of the theory. First we note that the counter-term $\delta\lambda_{\rm et}$ in figure 15 is equal to the counter-term $\delta\lambda_{\rm bb}$ in equation (41) at the 1-loop level, since we can replace the bare vertex with the proper one when working at 1-loop.

At 2-loops these counter-terms will not be the same. This is because the integral equation for the vertex V obtained from the n-Loop nPI effective action contains terms up to $n-3$ loops, while the corresponding equation for Λ_f contains up to $n-2$ loops (these results follow from the fact that functionally differentiating a graph with respect to V opens 3 loops, and differentiating with respect to G opens 1 loop). Therefore, in order to compare the counter-terms that renormalize these two 4-point vertices, we must compare the Λ obtained from the 4-loop 4PI effective action, and the V equation of motion obtained from the 5-loop 4PI effective action.

The 5-loop 4PI effective action in the symmetric theory contains only one additional diagram [14], which is shown in part (a) of figure 17. The corresponding contribution to the V equation of motion is shown in part (b) of the figure.

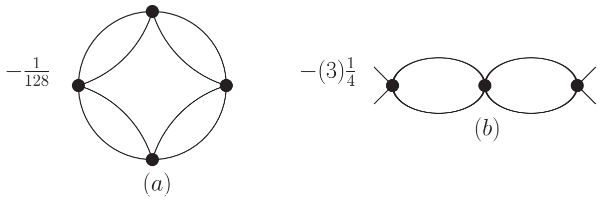

FIG. 17. The 5-loop skeleton diagram in the effective action and the corresponding contribution to the equation of motion.

From equation (38) we know that there is an overlapping divergence in this 2-loop contribution to the equation of motion, and it appears that there is no counter-term to cancel this overlapping divergence. However, we know that if we expand the equation of motion for the vertex V perturbatively, we will generate an infinite set of overlapping divergences and an infinite set of diagrams containing the counter-term $\lambda_{\rm bb}$. To show that the overlapping divergences cancel, we have to rearrange the equation of motion in a more convenient way. We use the M equation discussed in the previous section for guidance. We rewrite the 1-loop s- and t- u-channels by substituting the equation of motion into itself. This is shown in figure 18.

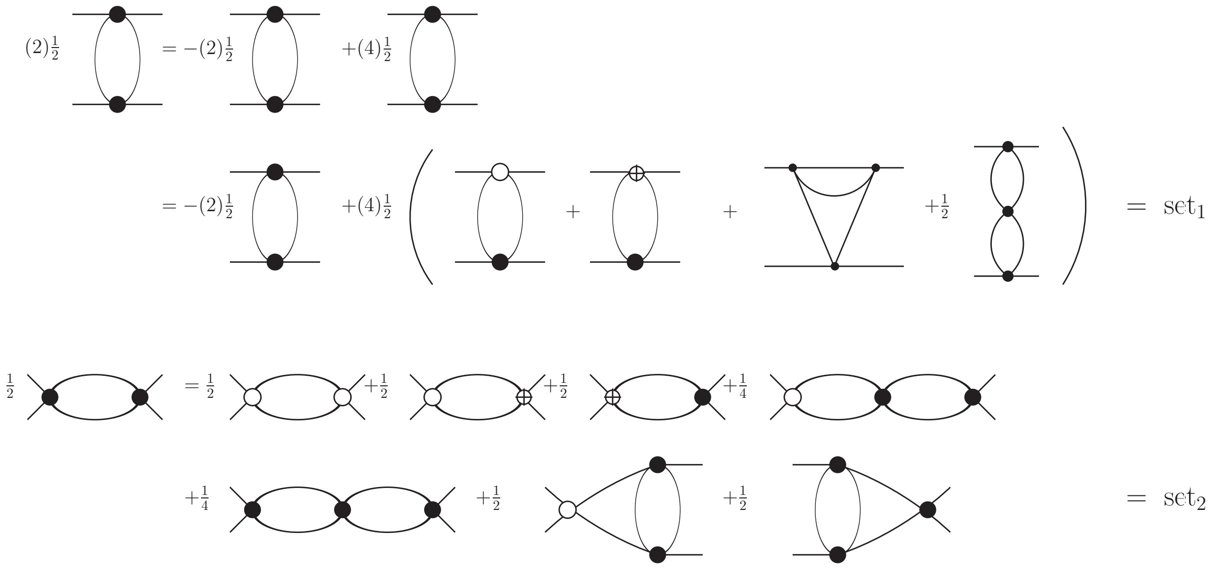

FIG. 18. Rearrangement of the 1-loop diagrams in the V equation of motion.

Combining 1-loop contributions to the equation of motion we have:

$$V^{(1)} = \delta\lambda^{(1)}_{\rm bb} + {\rm set}_1\Big|_{1\,{\rm loop}} + {\rm set}_2\Big|_{1\,{\rm loop}} . \tag{79}$$

The 1-loop diagrams in set$_1$ and set$_2$ are, by construction, the same as the 1-loop diagrams in $m^{(1)}$ (see figure 10), and therefore we can use $\delta\lambda^{(1)}_{\rm bb} = \delta\lambda^{(1)}_{\rm et}$ (see equation (75) and figure 15) to renormalize the rearranged V equation of motion at the 1-loop level.

Now we look at the 2-loop graphs. As before, since we are working at the level of 2-loop skeleton diagrams in this section, we can set the bare vertex equal to the proper one in 2-loop diagrams. We insert the 1-loop counter-term $\delta\lambda^{(1)}_{\rm et}$ obtained from equation (75) (figure 15) with $V_0 = V$, which is just $-3/2 I_1(V_0, V_0)$ or $-3/2$ times the grey blob in the second diagram on the right side. Adding the contributions in figures 17(b) and 18 and collecting topologies we obtain the graphs in figure 19.

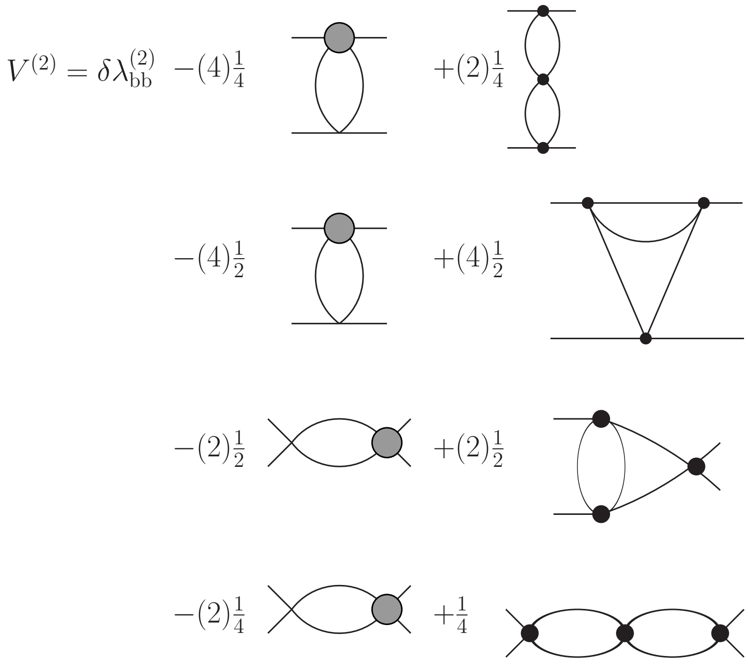

FIG. 19. The 2-loop diagrams in the V equation of motion.

All graphs which contain a grey blob are produced by substituting the 1-loop counter-term into a 1-loop topology in figure 18. The graphs with grey blobs in the first two lines come from the 1-loop t- u-channels (the third graph in the second line of figure 18), and the graphs with grey blobs in the third and fourth lines of figure 19 come from the 1-loop s-channel (the second and third graphs in the right side of the third line of figure 18). We have artificially divided these counter-term contributions into two pieces so that we can see explicitly the pattern of cancellation of the overlapping divergences. The coefficients of the vertical and horizontal triangle graphs on the right side of figure 19 are obtained directly from figure 18. The coefficient of the vertical double-scoop diagram in figure 19 is obtained from figure 18 and the t- u-channel parts of figure 17(b). Figures 17(b) and 18 contribute $-2\frac{1}{4}$ and $4\frac{1}{2}\frac{1}{2}$, respectively, and so total factor is $\frac{1}{2}$, which we write as $(2)\frac{1}{4}$ to indicate that the u-channel should be drawn separately. Similarly, the coefficient of the horizontal double-scoop is $-\frac{1}{4}$ from figure 17(b) and $\frac{1}{4}+\frac{1}{4}$ from figure 18, which gives $\frac{1}{4}$.

The diagrams on the right side of figure 19 can be divided into finite pieces, momentum independent divergences, and overlapping divergences using (27) and (38) (see figures 4 and 5). The overlapping divergences cancel and the momentum independent divergences can be cancelled by the counter-term $\delta\lambda^{(2)}_{\rm bb}$. Collecting terms we obtain $\delta\lambda^{(2)}_{\rm bb} = \delta\lambda^{(2)}_{\rm et}$ (see equation (78)).

Thus we have shown that if we calculate the vertex M from the 4-Loop 4PI effective action and the vertex V from the 5-Loop 4PI effective action, the counter-terms $\delta\lambda_{\rm et}$ and $\delta\lambda_{\rm bb}$ are the same at the 2-Loop level of the skeleton expansion.

VIII. NUMERICAL CALCULATIONS

In this section we calculate numerically the 2-point and 4-point functions in 2-dimensions. We work in Euclidean space and redefine the variables:

$$\lambda = -i\lambda_E\,,\quad \delta\lambda = -i\delta\lambda_E\,,\quad V = iV_E\,,\quad G = -iG_E\,,\quad \Sigma = -i\Sigma_E\,. \tag{80}$$

In this section all variables are Eucledian and we suppress the subscript E. Note that in 2-dimensions the coupling constant and 4-point vertex have dimension 2 (and not 0 as in 4-dimensions).

We will solve the self-consistent equation of motion for the 2- and 4-point functions using a numerical lattice method. For comparison, we start by looking at the corresponding perturbative calculation in two dimensions. For the 4-point function the diagrams we need are obtained from figure 6 with proper vertices replaced by bare ones. In 2-dimensions there are no ultraviolet divergences in these 1-loop diagrams, and therefore we can set the counter-term $\delta\lambda_{\rm bb}=0$. From equations (39) and (40) one can show that the 4-point vertex to order λ^2 is given by:

$$\begin{aligned} V(P_a,P_b,P_c) = -\lambda + \frac{\lambda^2}{8\pi}\int_0^1 dx\Big[&\frac{1}{m^2+x(1-x)(P_a+P_c)^2} \\ &+\frac{1}{m^2+x(1-x)(P_a+P_b)^2}+\frac{1}{m^2+x(1-x)(P_b+P_c)^2}\Big]+\mathcal{O}(\lambda^3)\,. \end{aligned} \tag{81}$$

The diagrams we need for the 2-point function are shown in figure 20.

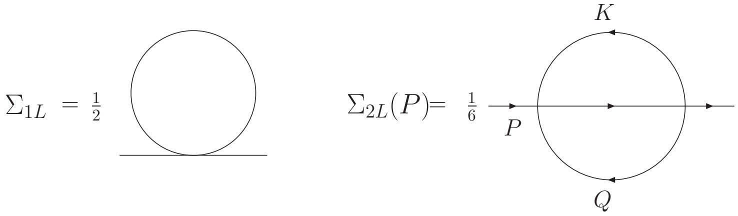
Σ_{1L} = $\frac{1}{2}$
$\Sigma_{2L}(P)$= $\frac{1}{6}$
K
P
Q

FIG. 20. 1-loop and 2-loop self-energy diagrams in perturbation theory.

A simple calculation gives the 1-loop self-energy:

$$\Sigma_{1L} = \frac{\lambda}{8\pi}\Big(\frac{1}{\varepsilon}-\gamma_E+\ln 4\pi+\ln\frac{\mu^2}{m^2}\Big)\,, \tag{82}$$

where μ is a mass scale introduced by dimensional regularization. Σ_{1L} is logarithmically divergent, but the divergence is independent of the external momentum. The 2-loop self-energy Σ_{2L} is also easily obtained as:

$$\Sigma_{2L}(P) = -\frac{\lambda^2}{6(4\pi)^2}\int_0^1 dx\int_0^1 dy\frac{1}{[y+(1-y)x(1-x)]m^2+y(1-y)x(1-x)P^2}\,. \tag{83}$$

Although the 2-loop self-energy Σ_{2L} is a function of the external momentum, it does not have an ultra-violet divergence in 2-dimensions. The inverse propagator is obtained from the self-energy as:

$$\begin{aligned} G^{-1}(P) = {}& P^2+m^2 \\ &-\frac{\lambda^2}{6(4\pi)^2}\int_0^1 dx\int_0^1 dy\frac{1}{[y+(1-y)x(1-x)]m^2+y(1-y)x(1-x)P^2}+\mathcal{O}(\lambda^3)\,. \end{aligned} \tag{84}$$

It can be renormalized by setting δZ=0 and choosing δm^2 to absorb the constant divergence in Σ_{1L} (see equation (10)).

The structure of the non-perturbative 4PI calculation is similar. The equation of motion for the 4-point vertex is shown in figure 6. The loop diagram is finite in two dimensions, and we drop the counter-term $\delta\lambda_{\rm bb}$. The equation for the 2-point function can be obtained directly from equations (11) and (42). The result is shown in the first line of figure 21. The diagrams can be rearranged by substituting the V equation of motion into the vertex on the left side of the sixth diagram. This substitution cancels the 3-loop diagram and produces the result shown in the second line of the figure.

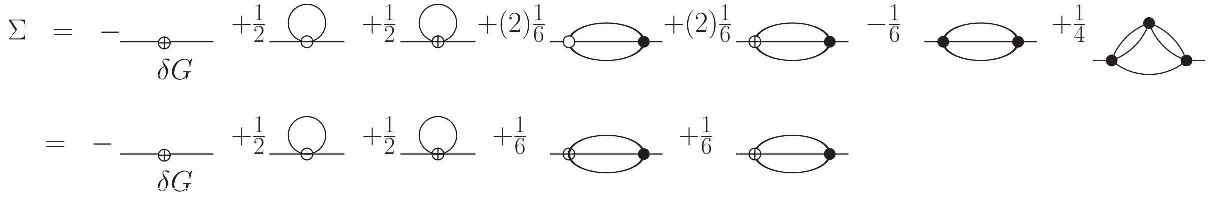

FIG. 21. The self-energy obtained from equations (11) and (42).

The 1-loop self-energy contains one momentum independent divergence from the tadpole diagram which can be absorbed by δm^2 . The 2-loop sunset diagram is finite in two dimensions, which means that we can choose $\delta Z = 0$ and drop the tadpole and sunset counter-terms in figure 21.

We use a $N \times N$ two dimensional symmetric lattice with periodic boundary conditions. The lattice spacing is a. In Euclidean space, the momentum is discretized:

$$p_i = \frac{2\pi}{aN} n_i \, (i = 1, 2), \quad n_i = -\frac{N}{2} + 1, ..., \frac{N}{2} \,. \tag{85}$$

On the lattice, the equation of motion for the 4-point vertex (equations (39) and (40)) is transformed into:

$$\begin{aligned} V(P_a, P_b, P_c) = -\lambda + \frac{1}{2}\frac{1}{(aN)^2}\sum_Q \Big[& V(P_a, P_c, Q)G(Q)G(Q + P_a + P_c)V(P_b, P_d, -Q) \\ & + V(P_a, P_b, Q)G(Q)G(Q + P_a + P_b)V(P_c, P_d, -Q) \\ & + V(P_a, P_d, Q)G(Q)G(Q + P_a + P_d)V(P_b, P_c, -Q) \Big] \,. \end{aligned} \tag{86}$$

The 2-loop self-energy on the lattice is easily obtained from figure 21 as:

$$\Sigma(P) = \frac{\lambda}{6}\frac{1}{(aN)^4}\sum_Q \sum_K V(P, Q, K)G(Q)G(K)G(Q + K + P) \,. \tag{87}$$

The gap equation in Euclidean space is:

$$G^{-1}(P) = G_0^{-1}(P) + \Sigma(P) \,. \tag{88}$$

Figure 22 shows the 4-point vertex and the self-energy as functions of the coupling strength λ, calculated from 4PI effective action and perturbation theory, where we choose the external momenta to be vanishing. The lattice spacing $a = 2\pi/(Nm)$ is adopted and two values of lattice number $N = 16$ and $N = 8$ are used. When the coupling strength is small, for example when λ is less than $2m^2$, the results obtained from 4PI calculations are consistent with the perturbative ones, for both the vertex and the self-energy. However, when the coupling constant becomes large, the perturbative results are quite problematic, as shown in the left panel of figure 22, where the 4-point vertex changes sign at large λ. This behaviour does not occur in the non-perturbative result.

In figures 23 and 24, respectively, we show the dependence of the 4-point vertex $V(P_a = P, P_b = 0, P_c = 0)$ and the self-energy on the external momentum. We look at several values of the coupling constant. Calculations are performed both in the 4PI formalism and in the perturbation theory. We observe again that the 4PI calculations are consistent with the perturbation ones when the

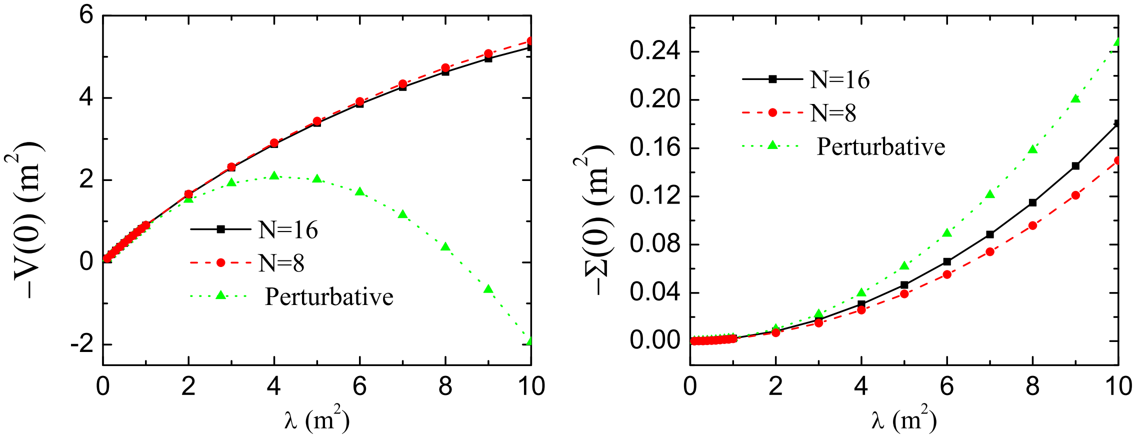

FIG. 22. (color online). Left panel: Comparison of the 4-point vertex with external momenta vanishing as a function of the coupling strength λ, obtained from the 4PI numerical study and perturbative calculations. For the 4PI calculation, we use lattice spacing $a = 2\pi/(Nm)$ and two values of the lattice number $N = 16$ and $N = 8$. Right panel: Self-energy with external momentum zero as a function of the coupling strength.

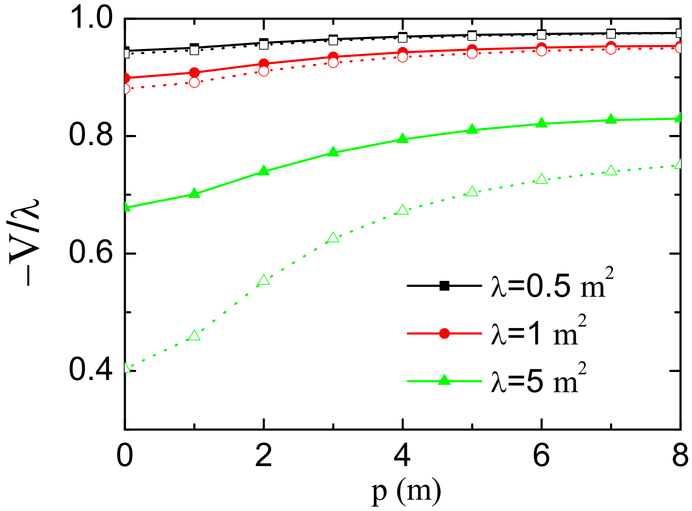

FIG. 23. (color online). Dependence of the 4-point vertex $V(p_a = p, p_b = 0, p_c = 0)$ on the external momentum. Results are shown for perturbation theory and using the 4PI effective action formalism. We use lattice spacing $a = 2\pi/(Nm)$ and $N = 16$ for the 4PI calculations.

coupling is small. However, the discrepancies between the two calculations become more and more pronounced as the interaction strength increases.

As a final comment we note that the full momentum dependence of the 4-point vertex can be obtained in the 4PI effective action formalism from equation (86). In figure 25, we give a contour plot of the 4-point vertex which depicts the dependence of the vertex on two momentum components. One can see that the vertex has a minimum at the origin of the coordinates, and the gradient varies with a change of direction.

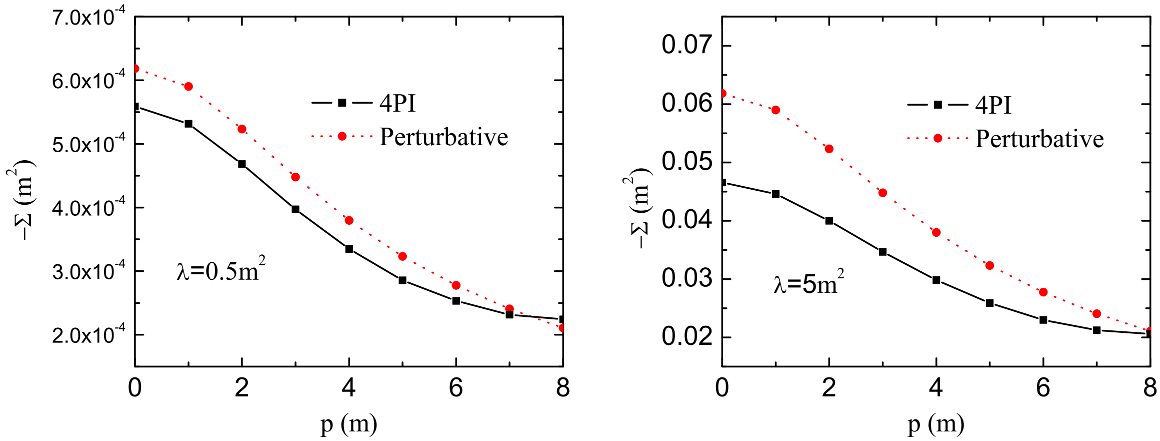

FIG. 24. (color online). Dependence of the self-energy on the external momentum with $\lambda = 0.5m^2$ (left panel) and $\lambda = 5m^2$ (right panel). Results are shown for perturbation theory and the 4PI effective action formalism. We choose lattice spacing $a = 2\pi/(Nm)$ and $N = 16$ for the 4PI calculations.

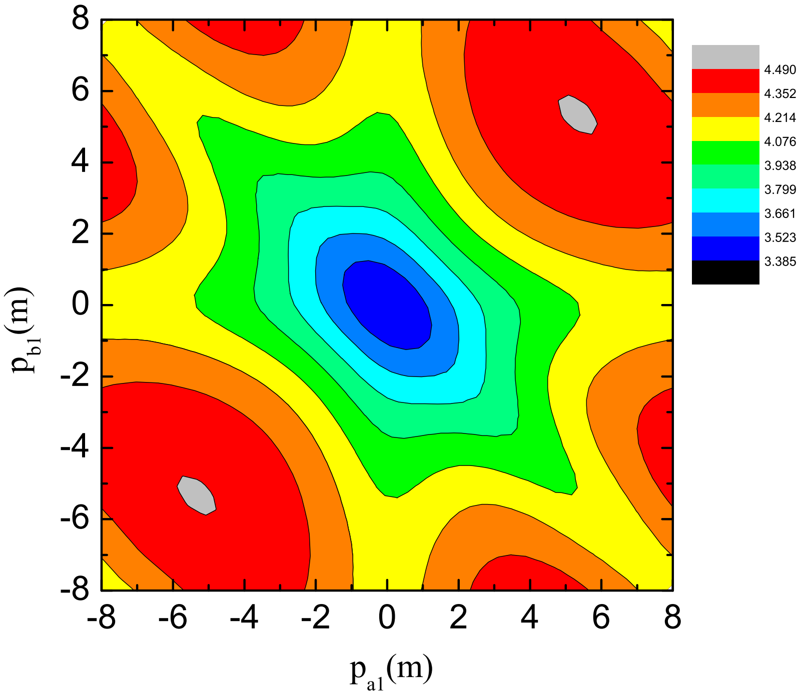

FIG. 25. (color online). Contour plot of the 4-point vertex $-V(p_{a1}, p_{b1})$ with other momenta vanishing. We use $\lambda = 5m^2$, $a = 2\pi/(Nm)$ and $N = 16$.

IX. SUMMARY AND OUTLOOK

In this paper we have demonstrated the renormalizability of the self-consistent 2- and 4-point functions obtained from the 4-Loop 4PI effective action. We have shown that the counter-terms that renormalize these functions are the same, up to the level of the truncation of the effective action. The equation of motion for the proper vertex V is symmetric in the three Mandelstam channels, whereas the vertex Λ contains only the t- and u-channels. The divergences in the 2-point function can be packaged into another vertex M which resumms Λ in the s-channel. The vertex M calculated from the 4-loop 4PI effective action has the same structure as the vertex V calculated from the 5-Loop 4PI effective action, and the two vertices are renormalized using the same counter-term $\delta\lambda$ on both the EIGHT and BBALL$_0$ diagrams in the original effective action.

As an indication of the usefulness of the 4PI effective theory, we have solved the integral equations in 2-dimensions using numerical lattice calculations. We have compared our results with those obtained in perturbation theory when the coupling strength is small and perturbative calculations are reasonable. The two calculations are in good agreement in the perturbative region. When the coupling is large, perturbation theory is not applicable, and the results of the perturbative calculation are not sensible. The 4PI effective action theory is a non-perturbative method which can be used consistently when the coupling is large. The full-momentum dependence of the 4-point vertex is easily obtained in the 4PI formalism.

We have only performed numerical calculations in two dimensions, and it would be interesting to extend the calculation in this paper to four dimensions. It would also be of interest to calculate a physical quantity like the pressure or shear viscosity using the 4PI effective theory. Work in these directions is in progress.

ACKNOWLEDGEMENTS

This work was supported by the Natural and Sciences and Engineering Research Council of Canada and by the National Natural Science Foundation of China under Contracts No. 11005138.

---

[1] E. Braaten and R. D. Pisarski, Nucl. Phys. **B 337**, 569 (1990).
[2] J. M. Luttinger and J. C. Ward, Phys. Rev. **118**, 1417 (1960); G. Baym and L. P. Kadanoff, Phys. Rev. **124**, 287 (1961); P. Martin and C. De Dominicis, J. Math. Phys. **5**, 14 (1964); **5**, 31 (1964).
[3] J. M. Cornwall, R. Jackiw, and E. Tomboulis, Phys. Rev. **D 10**, 2428 (1974).
[4] J. P. Blaizot, E. Iancu, and A. Rebhan, Phys. Rev. Lett. **83**, 2906 (1999), arXiv:hep-ph/9906340; Phys. Rev. **D 63**, 065003 (2001), arXiv:hep-ph/0005003.
[5] J. Berges, Sz. Borsányi, U. Reinosa, and J. Serreau, Phys. Rev. **D 71**, 105004 (2005),arXiv:hep-ph/0409123.
[6] J. Berges and J. Cox, Phys. Lett. **B 517**, 369 (2001), arXiv:hep-ph/0006160; J. Berges, Nucl. Phys. **A 699**, 847 (2002), arXiv:hep-ph/0105311; G. Aarts and J. Berges, Phys. Rev. Lett. **88**, 041603 (2002), arXiv:hep-ph/0107129; G. Aarts, D. Ahrensmeier, R. Baier, J. Berges, and J. Serreau, Phys. Rev. **D 66**, 045008 (2002), arXiv:hep-ph/0201308.
[7] J. P. Blaizot, J. M. Pawlowski, and U. Reinosa, Phys. Lett. **B 696**, 523 (2011), arXiv:1009.6048 [hep-ph].
[8] G. Aarts and J. M. Martínez Resco, JHEP **02**, 061 (2004), hep-ph/0402192.
[9] J. Berges, Phys. Rev. **D 70**, 105010 (2004), arXiv:hep-ph/0401172.
[10] G. D. Moore, Proceedings of SEWM 2002, Ed. M.G. Schmidt, arXiv:hep-ph/0211281.
[11] M.E. Carrington and E. Kovalchuk, Phys.Rev. **D77**, 025015 (2008), arXiv:0709.0706 [hep-ph].
[12] R. E. Norton and J. M. Cornwall, Ann. Phys. (N.Y.) **91**, 106 (1975).
[13] M.E. Carrington, Eur. Phys. J. **C35**, 383 (2004),arXiv:hep-ph/0401123.
[14] M. E. Carrington and Y. Guo, Phys. Rev. **D 83**, 016006 (2011), arXiv:1010.2978 [hep-ph].
[15] M. E. Carrington and Y. Guo, arXiv:1109.5169 [hep-ph].
[16] M. E. Carrington and E. Kovalchuk, Phys. Rev. **D 80**, 085013 (2009).
[17] M. E. Carrington and E. Kovalchuk, Phys. Rev. **D D81**, 065017 (2010), arXiv:0912.3149 [hep-ph].
[18] D. Binosi and L. Theussl, Comput. Phys. Commun. **161**, 76 (2004), arXiv:hep-ph/0309015.
[19] J. Berges, Sz. Borsányi, U. Reinosa, J. Serreau, Annals Phys. **320**, 344 (2005), arXiv:hep-ph/0503240.